



Predisposing factors and hydrodynamic conditions controlling the failure of earth dams by overtopping based on physical modeling experiments

Dongxia Yue¹ · Yongbin Wang¹ · Liangsheng Zhao¹ · Yan Chong¹ · Guan Chen² · Xingmin Meng²

Received: 4 December 2023 / Accepted: 3 July 2024 / Published online: 5 August 2024
© The Author(s) 2024

Abstract

Dam landslides occurred frequently during recent years, and the secondary disasters caused by it can cause great harm to local resident in an extensive area. Therefore, it is important to understand the mechanisms of dam failure. Experiments were designed to study the mechanisms of dam failure, analyze the effects of multi-factors, and establish a method for the critical condition of dam breach. The results showed that before the collapse, the existence of the notch surface accelerates infiltration and causes advancement of the speed of the wet front. The dam failure process can be divided into three stages: erosion initiation, erosion acceleration, and erosion weakening. During the breaching, three important erosion phenomena were observed including slope instability, steep slope, and collapse. Based on statistical analyses of the changes in the longitudinal slope profile and erosion rates observed during the dam failure, characteristics of erosion rate along the longitudinal profile have been summarized well. The slope of the bottom groove, size of the dam body, upstream inflow discharge, and median particle size of the dam body significantly affected the characteristics of the dam body collapse. Then, a critical water head that leads to an overtopping outburst was established based on the experimental data and theory of incipient motion of sediment, providing critical information to predict dam failure. The results of this research would be helpful to predict the disaster chain and enhance the risk management of this kind of disaster chain.

Keywords Landslide dam · Overtopping · Evolution process · Impact factors

Introduction

Many factors, such as excessive rainfall, earthquakes and river erosion, lead to the distribution of landslides in the river bed. These landslides can enter river channels and choke rivers, forming a type of river blockage called a natural dam (Takahashi 2007). Natural dam formations

are common disasters in mountainous regions worldwide (Korup 2002; Casagli et al. 2003; Cui et al. 2013; Chen et al., 2015; Jiang 2019). For example, the 2008 Wenchuan earthquake in China produced tens of large (with volumes greater than 1 million m³) rock avalanches (Wasowski et al. 2021), many of which resulted in dangerous landslides and produced numerous natural dams. Over 50% of natural dams break by overtopping, and 85% fail within one year of formation (Costa et al. 1988). Dams formed by river blockages from landslides, collapses, and debris flows often have very short lifespans and can induce a series of secondary disasters by triggering regional large-scale geological disaster chains. These natural disasters can cause great harm to large-scale water conservancy projects, highways, waterways, hydro-power facilities, and other infrastructures along the disaster chain. Therefore, it is important to understand the mechanisms of dam failure and predict potential dam breaches.

At present, physical experiments are the most common research method to study dam failures. Modeling experiments are generally based on the application of a certain

✉ Dongxia Yue
dxyue@lzu.edu.cn

Guan Chen
gchen@lzu.edu.cn

Xingmin Meng
xmmeng@lzu.edu.cn

¹ MOE Key Laboratory of Western China's Environmental Systems, College of Earth and Environmental Sciences, Lanzhou University, Lanzhou 730000, Gansu, China

² School of Earth Sciences, Lanzhou University, Lanzhou 730000, Gansu, China

weir dam as the dam prototype and seek to understand the failure process by controlling influencing variables. This method can effectively avoid the interference of multiple factors in the field and optimize statistical results. Previous research using these physical experiments has studied the influence of inflow rate and physical parameters of the dam (such as the particle size distribution of dam material and the shape of the dam) on the outburst process caused by overtopping and erosional characteristics (Hakimzadeh et al. 2014; Rifai et al., 2018; Jiang et al. 2020).

Additional research summarized the longitudinal evolution model of dam failure and developed a numerical model to characterize landslide dam failure from overtopping (Chang and Zhang 2010; Zhong et al., 2017, 2020; Zhou et al. 2019a, b). Although dam failures have been widely studied, the evolutionary process of dam failure is still not well-understood, especially regarding the dynamic process coupled with the lateral expansion of the breach. In addition, the dam collapse process is extremely complex, with numerous influencing factors. Most previous studies have focused on single-factor analyses, and there is a lack of research on the synergistic effects of multiple factors.

Quantifying the dam's stability and the critical conditions required for an outburst of the dammed lake is significant for early warning and prediction of outburst floods. Many studies have established relationships between dam stability, catchment area and slope of the main river, and volume and height of the dam through statistical analysis. From these analyses, a series of indices were proposed to quickly evaluate the stability of a dam (Ermini and Casagli 2003; Casagli et al. 2003; Iqbal et al. 2013; Stefanelli et al., 2013). Some studies have also analyzed the hydraulic conditions during a dam break and deduced formulas for the critical overflow depth, outburst flood velocity, and peak discharge (Jiang, 2008). However, due to the complex topography, geological environment, hydrological conditions, and material composition, the applicability of existing formulas for predicting dam stability is limited. Therefore, it is urgent to study the dynamic evolution and critical conditions of dam failure to provide a scientific basis for disaster prevention and reduction of the geological disaster chain.

A series of flume experiments were conducted in this study. A total of 8 simulation scenarios were designed based on a landslide-type natural dam prototype in Goulinping, characterizing a typical debris flow gully in a strong earthquake area in western China. Effects of multi-factors controlling the dam failures were analyzed, which includes the particle size, the flume bed slope, and the upstream inflow. Characteristics of erosion rate along the longitudinal slope profile were analyzed. Based on the understanding of failure mechanism and erosion characteristics, a formula of the critical water head for an overtopping breach was derived from theory of incipient motion of sediment. It is hoped that the

failure mechanism and critical condition of dam overtopped revealed in this study would be helpful for predictions of landslide dam failure, as well as quantitative evaluation and prediction of the effects of geological disaster chains in strong earthquake areas.

Experimental methods

Experimental setup

A large indoor flume at the Institute of Geological Natural Disaster Prevention, Gansu Academy of Sciences, China, was used to perform the experiments in this study. The flume consisted of a flat steel channel (7 m long, 0.5 m wide, and 0.8 m deep), The slope of the flume can be adjusted 0° to 20° . Three scenarios of 4° , 7° and 10° were set up in this experiment. The flume walls were made of transparent plexiglass to facilitate observations. A water tank with a volume of 2.6 m^3 was installed on top of the flume. We controlled the amount of upstream water entering the flume by adjusting the size of the water tank opening. The landslide dam was located above the middle of the flume (Fig. 1). A rectangular notch (0.05 m wide and 0.05 m deep) was opened on the side of the dam crest to control the location and process of each landslide dam failure. This method ensures that the overtopping failure starts at the same place every time, minimizing variability between different experiment runs (Zhou et al. 2019b).

Sensor layout

GS3 soil moisture temperature conductivity sensors (with a 0.1% resolution) were placed in different positions inside the dam to study the changes in water content that occur in different positions during the landslide dam failure process. GS3 soil moisture temperature conductivity sensors (DECA-GON METER Group) have a frequency of 70 MHz, a measurement speed of 150 ms with a 0.1% resolution. Fully meet the experimental requirements. As shown in Fig. 2(a) and (b), two observation surfaces were designed to arrange the sensors inside the dam. The observation surface 0.05 m away from the right-side glass was considered surface 1, with a rectangular recess at the top of the dam. The observation surface 0.2 m from surface 1 in the middle of the dam was considered surface 2, and there was no notch at the top of the dam at this position. Each dam contained 12 monitoring points, and 12 water content sensors were arranged at these monitoring points to monitor the changes in the soil water content during the dam failure. The layout of instruments on the sink device is shown in Fig. 2. A HYDRO-21 water level meter (resolution: 2 mm) and 6526 Doppler flow meter (resolution: 1 mm/s) were arranged upstream of the dam to

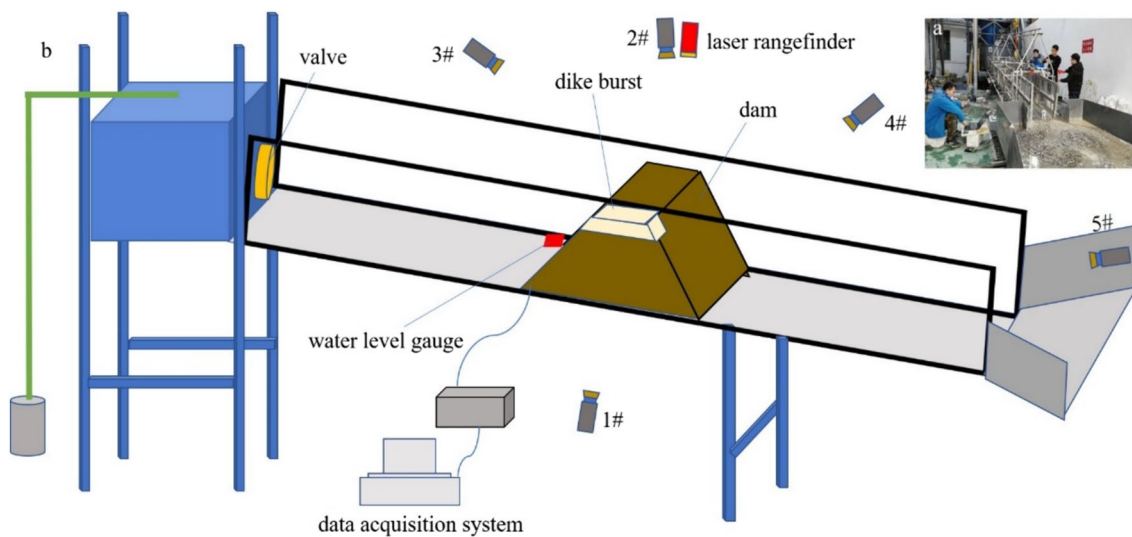


Fig. 1 Experimental setup (a) and layout of the observational setup: #1, #2, #3, #4, and #5 all indicate video cameras (b). Cameras #1 and #2 were used to photograph the morphological changes that occurred on the left and right sides of the dam in the failure process, respec-

tively. Cameras #3 and #4 were used to photograph the upstream and downstream slope changes of the dam, respectively. Camera #5 was used to observe the evolution of the flood or debris flow during the dam failure

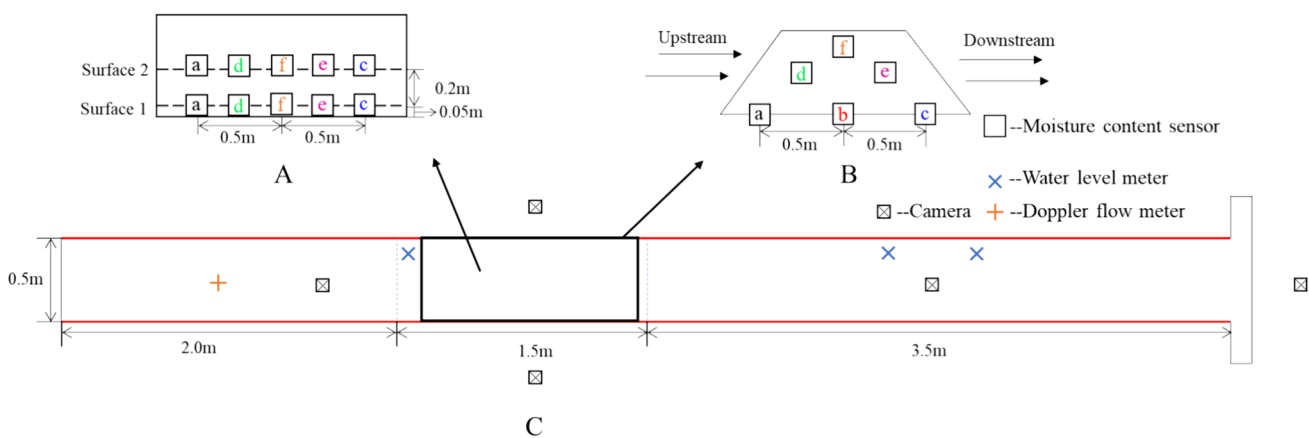


Fig. 2 Prone view map (a) and side view map (b) of the sensor layout in the dam. Prone view map of sensor layout in the flume device (c)

measure the front of the dam, the water levels before and after the dam failure, and the upstream flow.

Model design

The failure process of a barrier dam is affected by various factors, such as the local hydraulic conditions, the material composition of the dam, and the dam size. These control factors are key to studying the process and mechanism by which barrier dams fail. Taking a landslide dam formed in the Goulinping debris flow gully in 2019 as a prototype, a landslide dam model was designed at a scale of 1:50, and the inflow was designed at a scale of 1:50^{2.5} using geometric similarity theory. Goulinping Basin is located in Goulinping

Village, Jiaogong Town, Wudu District, Longnan City, Gansu Province. Its geographical coordinates are 103.6°E, 33.5°N, 3.2 km away from Wudu District, Longnan City. It belongs to the first-level tributary on the right bank of the middle reaches of Bailong River. Goulinping debris flow has the characteristics of high frequency and large scale, according to the field monitoring and measurement data, 28 large-scale debris flows occurred in Gulinping from 2013 to 2015. Because there are many potential landslides in the basin, the risk of forming the dam body still exists, so this paper has great scientific and practical significance.

The experimental design of this study was based on the proportional reduction principle, considering the dimensionless parameter set required so that the dam design conforms

to the geometric characteristics of the dam proposed by Peng and Zhang (2012). Peng and Zhang (2012) proposed put forward the main factors affecting the dam body: $\frac{H_d}{W_d}$, $\frac{V_D^{1/3}}{H_d}$ and $\frac{V_1^{1/3}}{H_d}$. Among them, W_d is the dam width, H_d is the natural dam height, V_d and V_1 are the volume of the dam and reservoir, respectively. According to the experimental design, $H_d = 0.5$ m, $W_d = 1.45$ m, $V_D = 0.194$ m³, $V_{14} = 0.59$ m³, $V_{17} = 0.58$ m³ and $V_{110} = 0.57$ m³. Therefore, $\frac{H_d}{W_d} = 0.34$, $\frac{V_D^{1/3}}{H_d} = 1.16$, $\frac{V_{14}^{1/3}}{H_d} = 1.18$, $\frac{V_{17}^{1/3}}{H_d} = 1.16$, $\frac{V_{110}^{1/3}}{H_d} = 1.14$. The above coefficient can meet the range requirements proposed by Zhou et al. (2019a, b), so it can meet the test requirements.

The experimental materials in this study were taken from the sudden deposits of a typical landslide in Gulinping catchment (Fig. 3). The main materials were limestone and phyllite, with a dry density of 1.8–2.0 g/cm³ and a porosity of about 25%. And the initial water content was controlled at about 4.5%. During the construction of the dam body, layer by layer is used to ensure that the porosity and density are consistent with the natural conditions.

Through field investigations and an analysis of the literature (LUKAS SCHMOCKER and WILLI H. HAGER., 2010; Cai et al. 2001; Yang and Cao 2012), we mainly studied the influence of four key control factors on the failure process of barrier dams. These factors were the slope of the flume, the flow of the upstream inflow, and the median diameter of the dam (Fig. 4). We strictly followed the controlled variable method during this study.

The experimental groups and parameters are shown in Table 1.

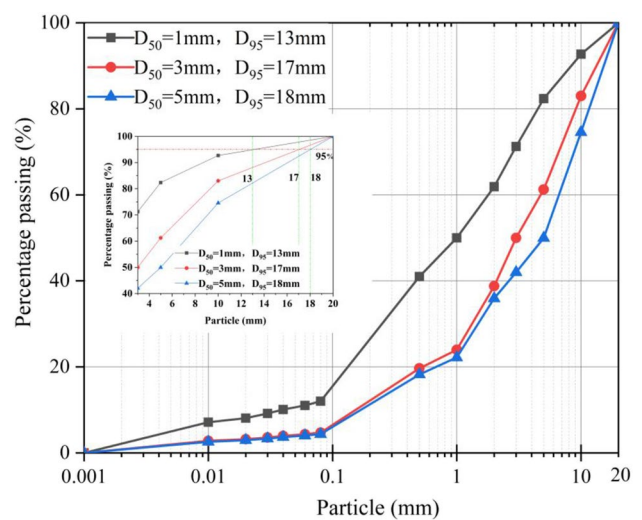


Fig. 4 Grain-size distributions of the experimental materials

The evolution of landslide dam failures

Video data containing the internal moisture content changes and surface (sidewall) contour deformation of each experimental dam were obtained by sensors and cameras, and the evolution of the dam collapse was analyzed. The experimental results revealed that the change process of the dam during dam failure was basically the same for each group. This change process could be roughly divided into three stages: erosion initiation, erosion acceleration, and erosion weakening. The following is a detailed analysis of the dynamic evolution of the No. 1 experiment.

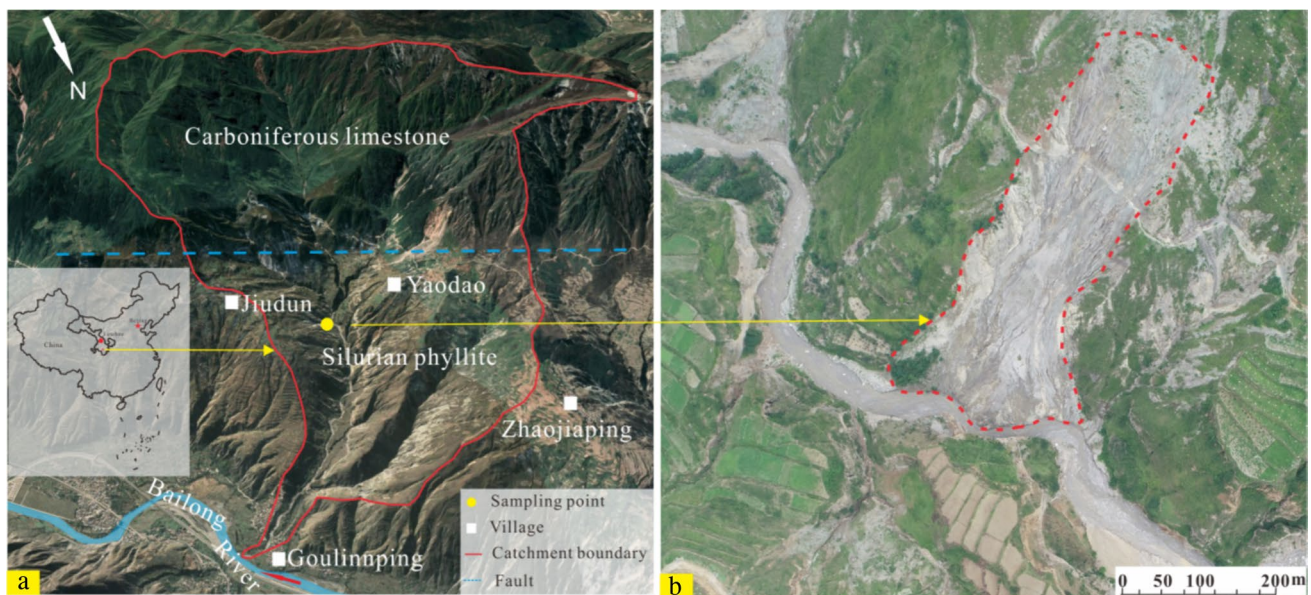


Fig. 3 Map of geographical location and sampling site of test samples in Gulinping Basin. Figure 3a is the location of the basin and the specific location of the sampling point in the basin; Fig 3b is a landslide in the basin and also the sampling point

Table 1 Experimental groups and parameters

Test NO	Length of top (m)	Length of bottom (m)	Width (m)	Height (m)	Initial water content	Inflow (m ³ /s)	d ₅₀ (mm)	flume bed slope	D ₉₅ (mm)
No. 1	0.1	1.45	0.5	0.5	<5%	0.0015	3	7°	17
No. 2	0.1	1.45	0.5	0.5	<5%	0.0015	5	7°	18
No. 3	0.1	1.45	0.5	0.5	<5%	0.005	5	7°	18
No. 4	0.1	1.45	0.5	0.5	<5%	0.0015	1	7°	13
No. 5	0.1	1.45	0.5	0.5	<5%	0.003	5	7°	18
No. 6	0.05	1.2	0.5	0.45	<5%	0.0015	3	7°	17
No. 7	0.1	1.45	0.5	0.5	<5%	0.003	5	4°	18
No. 8	0.1	1.45	0.5	0.5	<5%	0.003	5	10°	18

Moisture content changes inside the dam

As shown in Fig. 2(a) and (b), moisture content sensors were located at points a, b, c, d, e, and f of surface 1 (notch) and surface 2 (no notch) inside the dam. In Fig. 4, the color of the moisture content change curve is the same as that of the corresponding sensor point, and the main collapse stage is shown in shadow. Before the dam broke, a barrier lake gradually formed upstream of the dam. As such, this stage mainly involves water infiltration processes. Under the action of upstream water, the water movement comprised non-point source infiltration. The advancing processes of water infiltration and the wetting front were analyzed through the changes in water content with time, as indicated by the sensors.

During the experiment, the water content at the dam foot (point a) of the upstream slope on surface 1 (notch) first increased. The rise in water level in front of the dam was slower than the water infiltration process. The water contents in the middle (point b) and lower (point c) regions of the bottom of the dam rose first, and the soils in the upper and middle regions of the bottom of the dam reached saturation. At this time, the soil moisture abruptly moved horizontally. As the water level rose, the water content in the middle layer (point d) of the dam increased and reached saturation before that in the lower layer (point c).

According to Darcy's law, the soil water infiltration process is determined by the water potential gradient and the unsaturated hydraulic conductivity. With the passage of infiltration time, the effect of the gravitational potential in the vertical direction is more obvious. Therefore, at this stage, the moisture located at point d did not reach point e by gravity. Instead, this water first reached the bottom of the dam and flowed to point c along with the infiltrated water in the horizontal direction. Therefore, the soil at point c reached saturation after that at point d.

As the water level in front of the dam continued to rise, the soil at the bottom of the dam became saturated, and a complete seepage channel was formed at the bottom of the

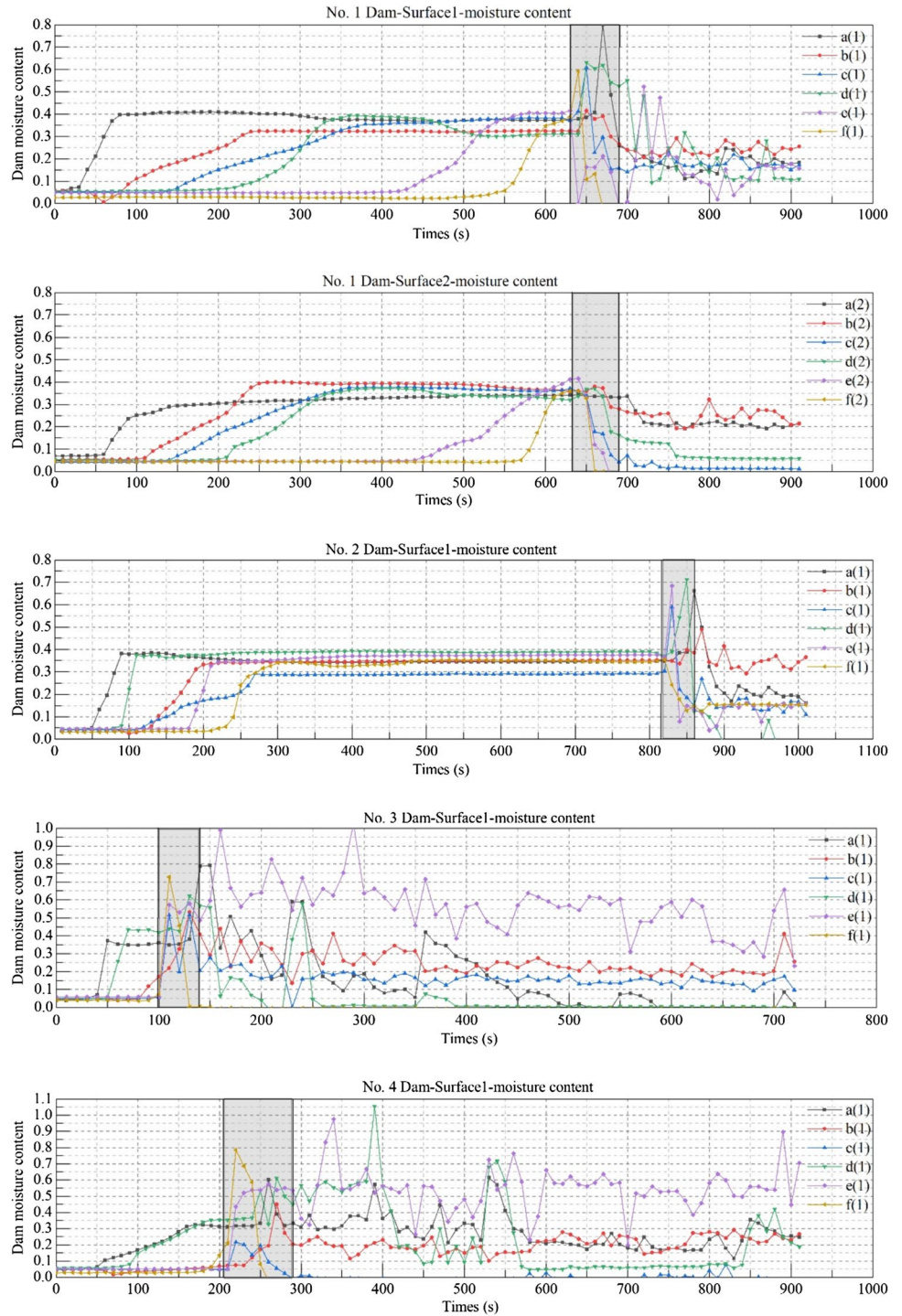
dam. At this time, the water diffused to point e, the water content at point e rose and reached saturation, and seepage also formed in the middle layer of the dam. Potential erosion damage due to seepage occurred in some areas of the downstream dam slope but did not affect the overall stability of the dam. With the gradual increase in the water level, the soil moisture content at the top of the dam (point f) finally reached saturation. Overall, the wetting front moved from the upstream slope to the downstream slope and from the bottom of the dam to the top.

The water content of experiment No. 2 (surface 2) showed the same trend as that of No. 1 (surface 1), but the increased rates of the soil water contents differed between the two surfaces. In surface 1, the water content of point a reached saturation first, while in surface 2, the water content of point b reached saturation first. These results indicate that the infiltration process of surface 1 was faster than that of surface 2, and the wetting peak of surface 1 also occurred faster than that of surface 2. The main reason for these differences is that surface 1 was closer to the right-side glass than surface 2, and this proximity hindered the lateral diffusion of water (Fig. 5).

Longitudinal evolution of dam failure

Figure 6 shows the longitudinal evolution of the dam failure in experiment No. 1. Four points, A, M, B, and P, were taken as representative points on the right side of the dam. Point A was located at the vertex of the upstream slope, point M was located at the midpoint of the dam crest, 0.05 m away from point B on the downstream slope crest, and point P was located at the midpoint of the downstream slope of the dam. Based on the above-described video data, a coordinate system was established by taking the bottom groove as the abscissa and the vertical line of point A at the top of the upstream slope as the ordinate to observe the longitudinal dam shape changes that occurred.

Fig. 5 Variation of the water content of the dam bodies during the experiments. Note: a(1) indicates point a of surface 1. The grey bars show the dam-breaking process

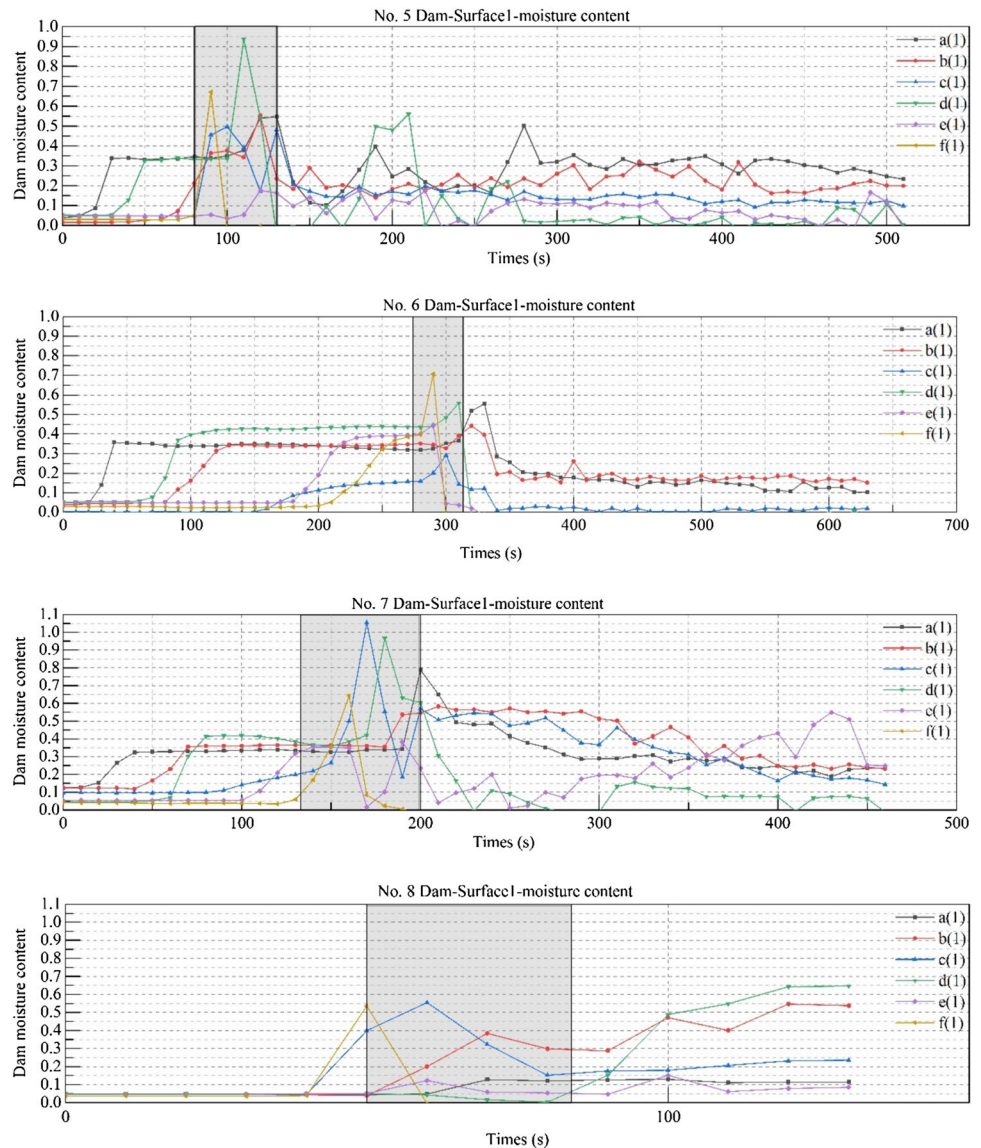


The time when the flow began to move along the initial gap to point B at the top of the downstream slope was set as the initial time, with t equal to 0 s. Point B was the location at which the overtopping collapse first occurred. The flow depth over the dam crest was still very shallow at this time, and the flow velocity was slow. These conditions were insufficient to erode the dam. In the initial stage of erosion (the first stage), point B of the dam was eroded by the water flow,

but the amount of erosion was small. Most of the eroded soils remained nearby and were mainly deposited on the downstream slope of the dam (in the area of point 'a').

When t was equal to 15 s, the flow mainly consisted of sediment flows, largely because the fine particles in the dam were easily eroded by the flow, increasing the number of suspended particles in the water. Before t was equal to 20 s, the geometric shape of the downstream slope

Fig. 5 (continued)



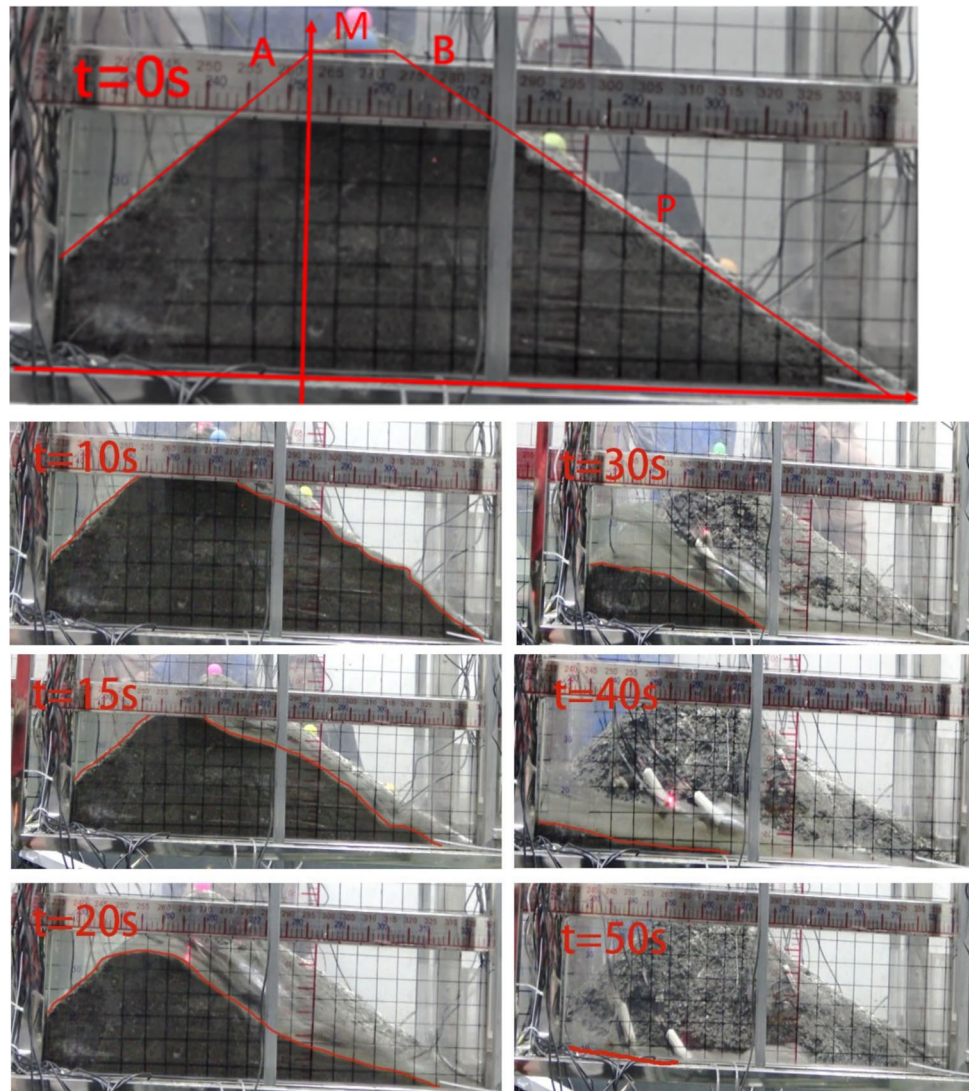
was relatively irregular. From 20 s onwards, erosion to the downstream slope began to accelerate, initiating the erosion stage (the second stage), and the top of the dam completely collapsed. With the increase in the amount of water released downstream, the erosion process of the downstream slope accelerated, and the downstream slope began to smooth due. At the same time, the flow caused erosion along its course and entrained soil particles, becoming turbid near the dam's foot. After t was equal to 30 s, in the stable, erosion weakening stage (the third stage), the residual material of the dam was reduced, the water level in front of the dam was low, the erosion rate had decreased, and sediment accumulated near the dam foot (the 'b' area) until the water level became close to the remaining dam height (Fig. 7).

A longitudinal evolution model of dam failure was established (Fig. 8) based on statistical analyses of the

longitudinal profile changes at each stage of the dam failure process obtained from the eight groups of experiments. To simplify the process, the irregular dam shapes attributed to the local geomorphologic changes caused by erosion and deposition were not considered. Instead, a smooth curve was used to replace the longitudinal profile of the dam at each time step. The term h_m is the maximum erosion height at each stage. B_c and W_d are the widths of the top and bottom of the dam, respectively. H_d is the height of the dam.

It can be seen from Fig. 8 that in the erosion initiation stage, the erosion point was initially located near the dam crest of the backwater slope of the dam body and gradually transferred to the dam crest. The erosion rate first increased and then decreased along the flow direction. In the accelerated erosion stage, the longitudinal profile of the dam body was similar to a spindle shape, and the erosion rate reached a maximum value near the vertex of the upstream dam

Fig. 6 Longitudinal snapshots of the dam failure process during experiment No. 1. The grid size on the window was $0.05\text{ m} \times 0.05\text{ m}$, and the red lines mark the surface profile of the dam



slope. The erosion rate first increased and then decreased along the flow direction. During the steady erosion stage, the location of the maximum erosion rate was transferred to the dam slope, and the erosion rate first increased and then decreased along the flow direction. Overall, the erosion rate first increased and then decreased along the flow direction. The maximum erosion point was traceable and reached a maximum value in the middle of the dam body.

Transverse evolution of dam failure

Taking the interface between the upstream or downstream dam slope and the bottom groove as the abscissa and the vertical direction of the slope surface as the ordinate, a coordinate system was established to represent the slope contour changes of the upstream slopes (Fig. 9(a)) and back slopes (Fig. 9(b)) of the dams at different times. The lateral evolution characteristics of the experimental dam failures

were summarized through observations of the upstream and downstream slopes' failure.

In the initial erosion stage, erosion began at the notch and gradually formed a retrogressive erosional process in the upstream slope. The downstream slope mainly experienced undercutting erosion, and the lateral change was small. Retrogressive erosion to the surface of the dammed lake quickly drained the water flow. In the accelerated erosion stage, the impact of hydrodynamic forces on the breach rapidly increased, and lateral and vertical erosion also increased. The soils on the sides of the breach collapsed, resulting in a narrow top and wide toe of the downstream slope. In the stable stage of erosion weakening, the scouring ability of the water flow was weakened, and the changes in the breach slowed. The erosion of the breach was mainly located on the sides of the breach. The bottom of the dam had a gap due to the action of the water flow. The upstream slope of the dam was wide at the top of the slope and narrow at the

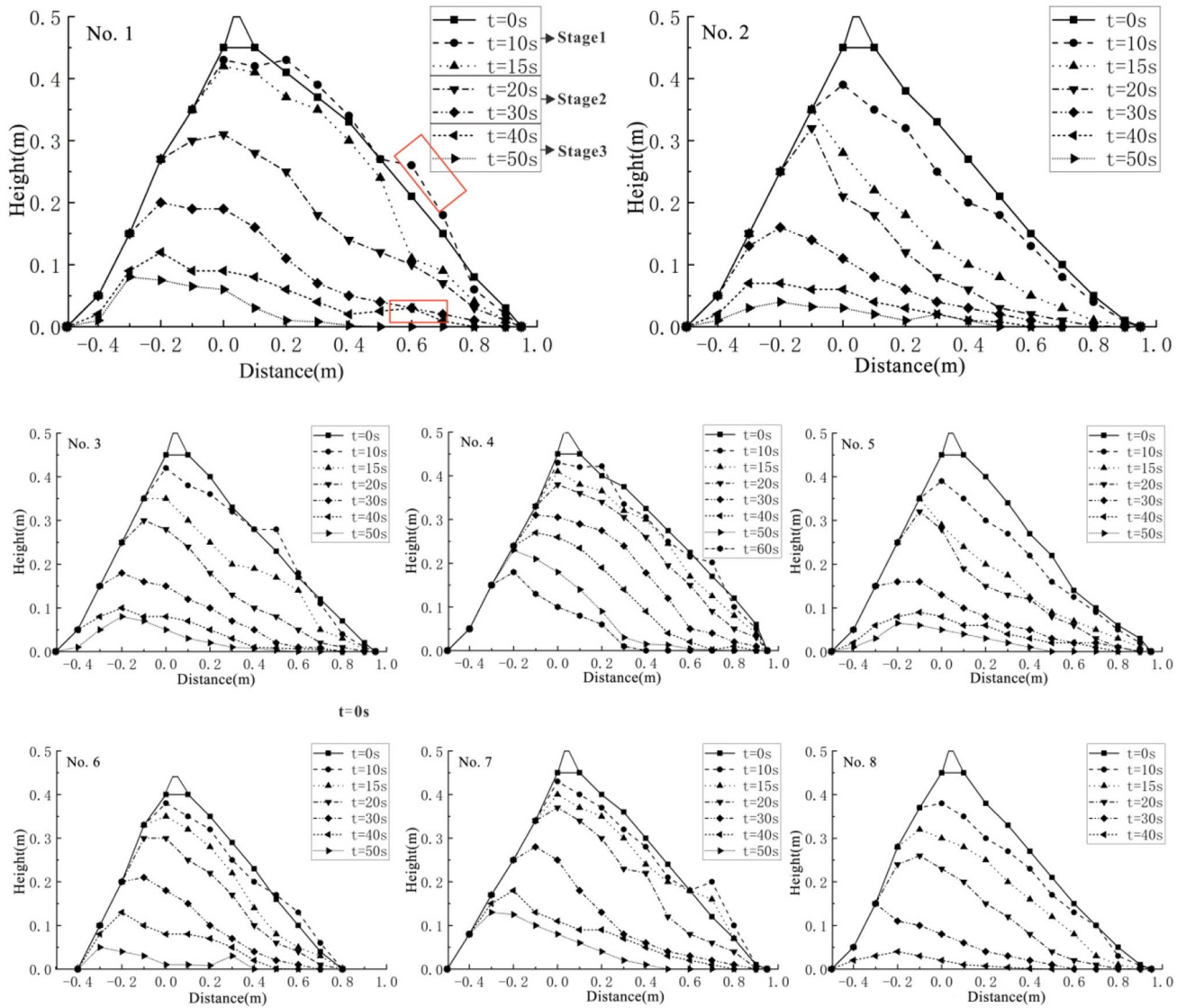
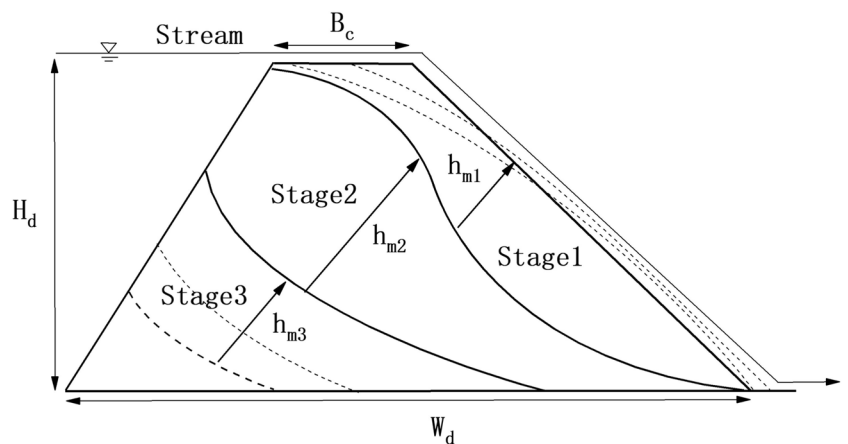


Fig. 7 Longitudinal profile changes in dam shape during experiments 1- 8

Fig. 8 Longitudinal evolution model of dam failure



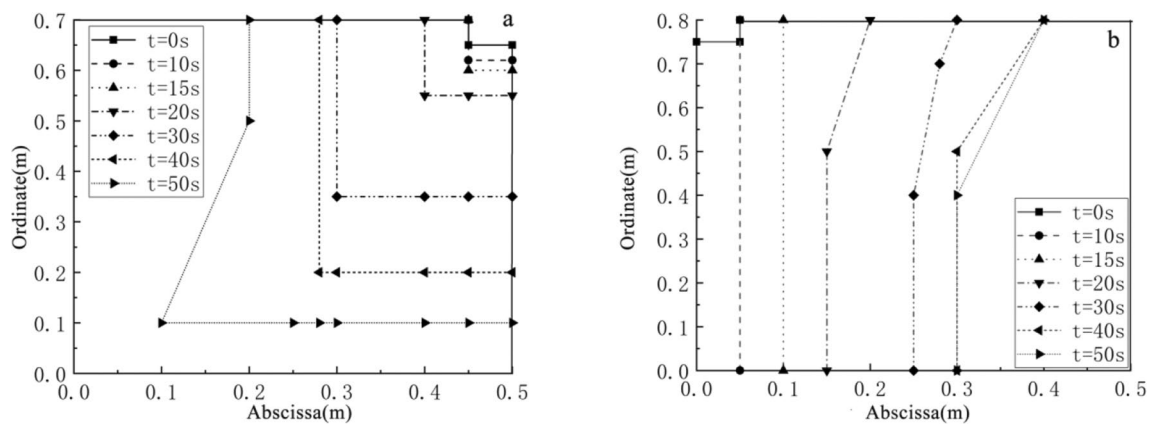


Fig. 9 Contour changes in the upstream slope (a) and downstream slope (b) at different times during experiment No. 1

toe of the slope. This process continued until the water flow was close to the height of the remaining dam. Comparing the change process of the water-facing slope with that of the downstream slope, it can be seen that the change in the downstream slope profile was large, and these changes mainly occurred in the erosion initiation stage and the accelerated erosion stage. The contour changes of the upstream slope mainly occurred in the accelerated erosion stage and the stable erosion stage. The collapse of the upstream slope lagged behind that of the downstream slope.

At the same time, through observing the downstream dam slope, it was found that three important erosion phenomena were involved in the experimental collapse process (Fig. 10). These processes include:

1.1. Slope instability: Due to the increase in infiltration in the dam body during the water storage process, the

downstream slope has a slight instability phenomenon (Fig. 10(a)), and the natural angle of repose at the lower part of the dam changes. However, this process is short, the change is not obvious, and the lower part of the dam soon restabilizes after the slope instability period. Therefore, this phenomenon will not destroy the integrity of the dam.

2.2. Steep slope (Zhu et al. 2011): In the dam failure process, a steep slope surface or a sloped surface with a certain inclination angle forms at the breach (Carrivick 2010), as shown in Fig. 10(b). At this time, the water flow does not move along the slope surface but directly impacts the bottom of the steep dam slope. With the erosion point retreating, a penetrating breach forms at the steep slope, accelerating the dam failure process.

3.3. Collapse: During the dam failure process, the stream flow does not cause layer-by-layer erosion but is

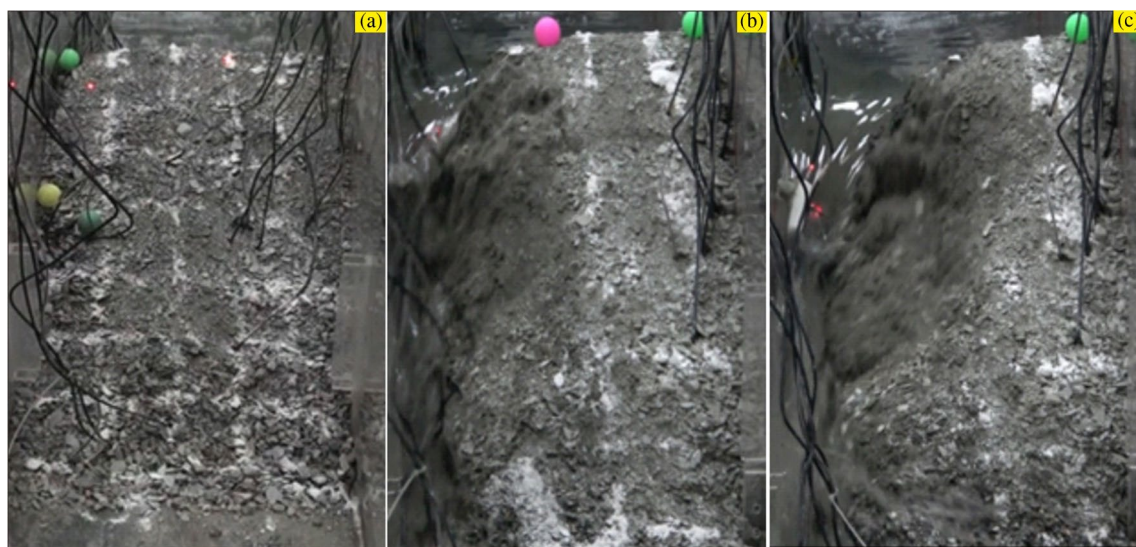


Fig. 10 a Slope instability; (b) steep slope; and (c) collapse erosion phenomena. The photos were taken during experiment No. 1

accompanied by the occurrence of the dam collapse (Fig. 10(c)). The rapid flow has a strong erosional effect on the soils on both sides of the dam, resulting in erosion of the lower soils and collapse of the upper part of the dam due to the lack of soil support.

According to the changing trend of the gap during the dam break, a transverse evolution model of dam failures was summarized (Fig. 11), in which H_d is dam height, L_d is dam length, and h_1 is the height at which the erosion point falls in stage 1.

The transverse evolution of dam failure can be divided into three stages. The first stage is the initial stage. In this stage, the main cause of lateral erosion of the dam body at this stage is water erosion due to the small flow velocity, weak erosional ability, and slow lateral expansion of the gap. The second stage is the rapid expansion stage. In this stage, the water flow velocity is high, the erosional ability is strong, and the lateral erosion rate is large. The main lateral erosion of the dam body during this stage is collapse and water flow erosion. The third stage is the stabilization stage. In this stage, the water flow decreases, the erosional effect of the water flow becomes weaker, and the slope gradient changes caused by the erosion effect are small. The residual dam body is basically stable, although some slope instability can still occur. The main cause of lateral erosion during this stage is lateral collapse.

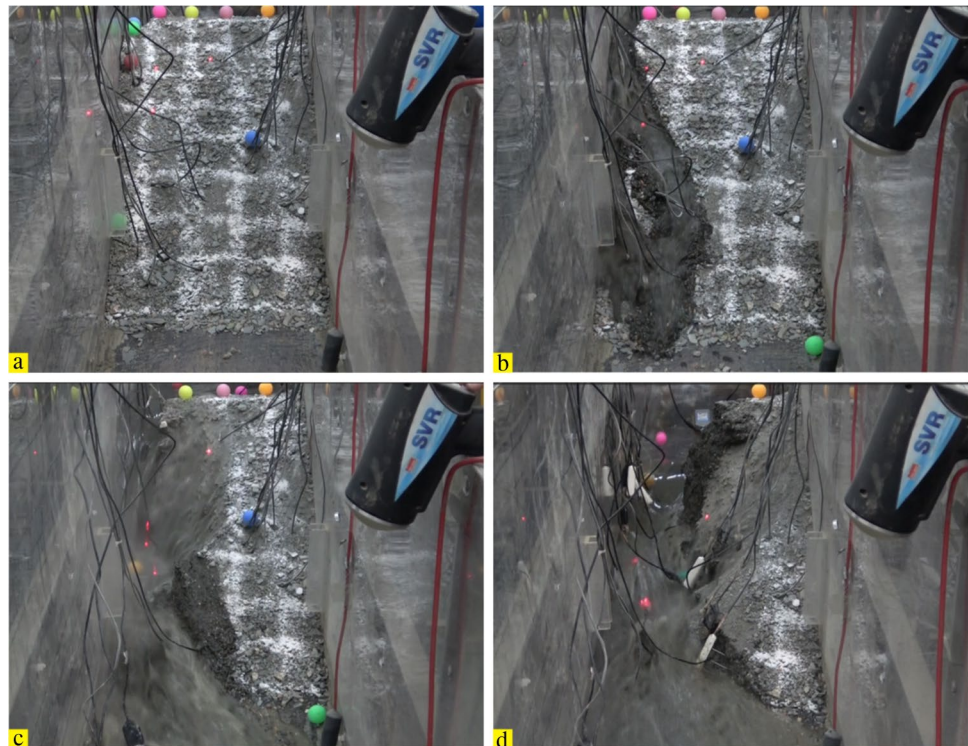
Variation of the outburst flow

The outburst flow is an important parameter of the dam burst, as it directly affects the degree of downstream damage of the burst flood. In this study, the change in the dammed volume was obtained by a water level gauge arranged at the bottom of the dammed lake in front of the dam. The burst flow was calculated from the water balance, and the burst flow curve was drawn according to the changing trend of the burst flow with time.

Analysis of the experimental burst flow hydrograph, combined with the horizontal and vertical erosion patterns during the dam burst process, led to the development of the change model of the outburst flow (Fig. 12). The overall process of the burst flow can be divided into three stages: Stage 1 is the stage of the slow growth of the burst flow. In this stage, the water flow overflows the preset burst and begins to erode the bottom of the preset burst and the backwater slope. The initial water flow is small and can only carry a small amount of soil downwards. During this stage, the outage flow gradually increases with time, but the growth rate is slow.

The second stage is the rapid growth and decline of the burst flow. In the first half of this stage, the growth rate of the burst flow becomes faster, and the burst flow rapidly increases to peak flow. In the second half of this stage, the burst flow decreases rapidly, and the dam body burst speed is accelerated. The collapse expands rapidly, and the collapse flow is large, but the duration is short. The third stage is

Fig. 11 The different stages of dam failure are as follows: **a** is the complete stage of the dam, **b** is the stage when the dam begins to be eroded, **c** is the stage when the dam begins to accelerate the erosion, and **d** is the stage when the dam is stable



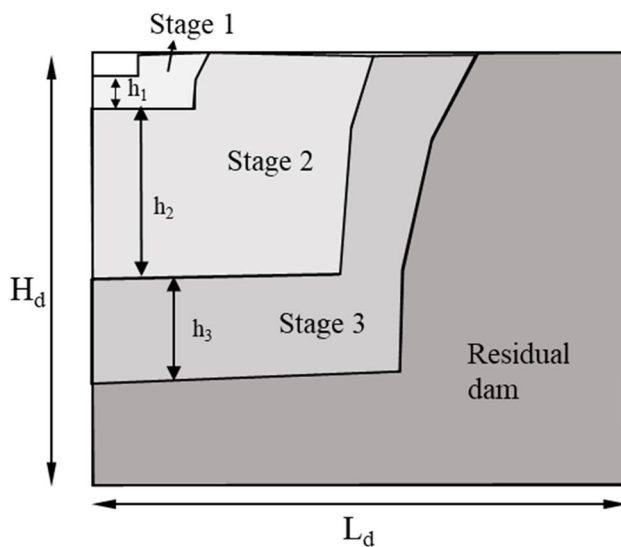


Fig. 12 Transverse evolution model of dam failure

the slow decline of the collapse flow. During this stage, the burst flow slowly decreases. The rate of decline gradually decreases until the flow finally equals the upstream inflow. At this time, the dam break process ends.

The influence of different control factors on the dam breach process

Our experiment focuses on the key control factors of dam failure. These factors are particle size distribution, upstream inflow discharge, the flume bed slope outburst flow, and the flume bed slope. The following sections discuss the influence of these factors in turn.

Influence of the particle size distribution on dam breaching

The characteristic diameter d_{50} and d_{95} were selected as one of the main control variables to study the impact of different particle size compositions on the dam failure process. Using the artificial soil screening method, the d_{50} values were set to 1 mm, 3 mm, and 5 mm as the screening standards, and d_{95} values set to 13 mm, 17 mm, and 18 mm.

The corresponding experimental numbers are No. 4, No. 1, and No. 2. By comparing the moisture content of different observed surfaces within the dam with these three mean grain diameters (Fig. 5), it can be seen that in the stage before the dam failure, the internal soil of the dam with a d_{50} value of 5 mm reached saturation at 200 s while the dam with a d_{50} value of 1 mm did not reach a saturated moisture content at the top of the dam before the dam failure. The middle and upper parts of the flume of the dam, with

a d_{50} value of 3 mm, only reached saturation at surface 1. The results show that the smaller the mean grain diameter, the weaker the permeability of the soil. The slower the wetting front moved, the smaller the saturated soil range. The reduced water infiltration greatly accelerated the speed of the water level rise, meaning that the water storage time before the dam collapsed was shorter in the experiments with less infiltration.

Comparing the longitudinal shapes and contour change maps of the experimental dams (Fig. 7 (No. 1/2/4)), it can be seen that the smaller the d_{95} value, the longer the failure process. During the first stage, the break position starts from the apex of the backwater slope of the dam body. When the d_{95} value of the dam body was 13 mm, the deformation of the backwater slope of the dam body was lowest, indicating the least amount of erosion. The dam body contour with a d_{95} value of 18 mm ended in the first stage. Later, the dam body began to become smooth due to the action of the water current. This result is because the smaller the d_{95} value, the more fine particulate matter. This fine particulate matter is susceptible to erosion by water, meaning that less material accumulates on the slope. The contour changes observed in the second stage of dam failure showed a similar pattern to those observed in the first stage. In the third stage, the dam body with a d_{95} value of 13 mm still had a 1.8-m-high water-facing slope that had not eroded in 50 s. In contrast, the dam bodies with d_{95} values of 17 mm and 18 mm were eroded at the feet of the water-facing slopes. The dam with a d_{95} value of 17 mm had more material remaining than the dams with the other d_{95} values.

Comparing the experiments with the different particle sizes and the same other conditions (No. 1/2/4), it was found that the smaller the median particle size, the higher the peak flow of the outburst produced by the dam failure. The flow hydrographs of the burst flow generated by the failure of each group of dam dams show that the shape of the curve gradually changed from thin and pointed to chunky with increasing median particle size. The particle gradation of the dam body affects its erosional resistance. The smaller the median particle size, the finer the dam particles, the weaker the erosion resistance, the shorter the burst time, the faster the burst flow rate, and the higher the burst flow peak value (Fig. 13).

Grains size distribution exerts a controlling influence on soil porosity and microstructure which will directly affect soil failure and flow (Li et al. 2015). Dueck et al. (2004) argued that smaller particle more higher combination by $E = Fad/dp$ (Fad is the adhesive force; dp is the particle diameter). Therefore, the soil permeability of small particles is poor. In addition, d_{50} plays a key effect on the stability of particles (Shu and Wang 2017), and fine particles are more easily transformed (Chen et al. 2010; Shen et al. 2022). Therefore the d_{50} effected the critical Shields stress

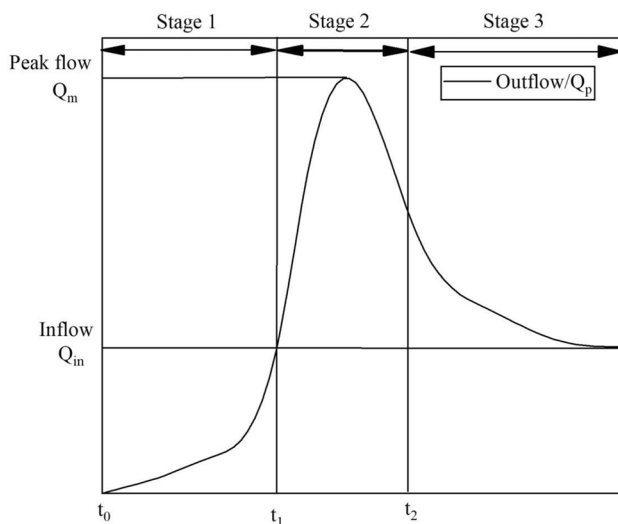


Fig. 13 The change model of the outburst flow

of sediment mixtures (Smith et al. 2023), so d_{50} is selected as one of the key parameter in this paper for experimental research. Meanwhile, Johnson et al. (2017) retrieves historical hydraulic conditions from d_{95} of sediments. Overall, it is clear that the particle size distribution plays a critical role in controlling dam failure.

Influence of upstream inflow discharge on dam failure

In our experiment, three kinds of upstream inflow discharges were designed to study their influence on the dam failure process. The manual adjustment method was used to alter the opening size of the water tank to control the flow rate. The Q_{in} values were set at 0.0016, 0.005, and 0.003 m^3/s , corresponding to experiment numbers No. 2, No. 3, and No. 5, respectively.

The moisture content curves of the dams with the three analyzed upstream flow rates are shown in Fig. 5 (No. 2/3/5). This figure shows that in the pre-dam failure phase, the Q_{in} value of 0.0016 m^3/s saturated the internal soil water content of the experimental dam when t was equal to 200 s, whereas the Q_{in} value of 0.003 m^3/s saturated the water content of the experimental dam only in the upper-middle part of the substrate before the dam failure. The experimental dam with a Q_{in} value of 0.005 m^3/s was only saturated in the upper part of the middle region and the upper part of the flume at surface 1. The discussion above stated that the particle size distribution affects the infiltration of the experimental material. In contrast, the greater the upstream flow, the less water infiltrated and the faster the water level rose. As such, the shorter the storage time before the dam collapsed, the slower the wetting front inside the dam and the smaller the

saturated soil extent. Therefore, the Q_{in} value is an important factor to evaluate and predict the time of dam overflow (Chen et al. 2017).

The changing shape profiles of the dam bodies (Fig. 7 (No. 2/3/5)) show that the smaller the upstream inflow, the slower the failure process. During phase 1, the dam failure always started at the top of the backwater slope of the dam. In the case of the experimental dam with a Q_{in} value of 0.0016 m^3/s , the initial failure stage was accompanied by sediment on the backwater slope. In the experiments with a Q_{in} value of 0.003 m^3/s and a Q_{in} value of 0.005 m^3/s , no material accumulation occurred in the initial stage of dam failure. This finding indicates that the larger the upstream flow, the more susceptible the backwater slope of the dam is to sediment accumulation.

Higher Q_{in} values increase the amount and range of erosion on the backwater slope material (Zhou et al. 2022). Higher flows and greater erosion are the prominent features in the longitudinal profiles in all three scenarios during the second phase. Interestingly, the remaining dam heights varied little among the three inflow categories. The highest remaining dam height occurred when Q_{in} was equal to 0.0016 m^3/s in the third stage. As the inflow discharge increases, the remaining dam heights gradually decrease. The water level in front of the dam was low and was mainly eroded by the kinetic energy of the water flow during this stage.

The outburst flow has a linear relationship with the outburst quantity (Frank Penner, 1987) and is also the energy source of secondary disasters (Zhu et al. 2019). By comparing the experiments with different upstream inflow and the same other conditions (No. 2/3/5), it was found that the larger the upstream inflow, the faster the rising rate of the burst flow, and the greater the peak value of the outburst flow. The outburst flow hydrographs of these different scenarios show that the larger the upstream inflow, the sharper the shape of the curve, and the larger the area of the polygon enclosed by the curve and the abscissa. The upstream inflow is a very important source of the burst flow. As such, the upstream inflow directly affects the total amount of water released by the dam failure. The larger the upstream water flow, the stronger the erosional ability, the faster the dam burst speed, and the larger the peak burst flow (Fig. 14).

Influence of the flume bed slope on the dam-breaking process

Three kinds of flume bed slopes were adopted to study the influence of the flume bed slope on the dam collapse process according to the middle and lower reaches of the Goulinping gully. The experimental numbers corresponding to flume slopes of 4°, 7°, and 10° are No. 5, No. 7, and No. 8,

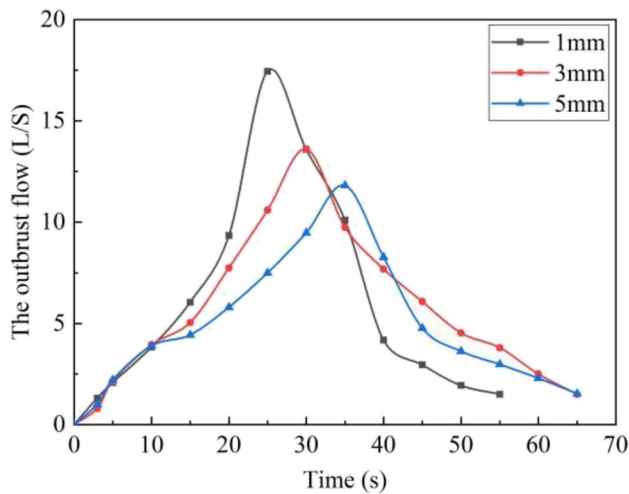


Fig. 14 Outburst flows under different particle size conditions (No. 1/2/4)

respectively. These flume slopes were achieved by manually adjusting the height of the flume bed.

Figure 5 (No. 5/7/8) shows the effect of the slope angle on the internal moisture contents of the dams, taking the condition of a 4° slope angle as an example. In the stage before the dam failure, the dam experienced approximately 150 s of water storage time, and the soil moisture content reached saturation except at the dam top. Viewed from other angles, however, the water content in the dam with a flume bed slope of 7° only reached saturation in the upper-middle part of the dam and the upper-middle part of the flume before the dam failure occurred. The dam with a flume bed slope of 10° did not reach saturation before water storage. The main reason for this result is that the larger the slope of the flume, the lower the water level in front of the dam. Under the same flow conditions, the shorter the water storage time before the dam breaks, the less water infiltration can occur. Further, the slower the movement of the wet front inside the dam, the smaller the range of saturated soil.

Figure 7 (No. 5/7/8) shows the effect of the slope angle on the longitudinal evolution of a dam failure. The larger the slope of the flume, the shorter the failure process time. During the first stage of the dam failure, the failure positions of the three types of flume slope experiments started from the apex of the land-side slope of the dam. The accumulation on the land-side slope was most obvious for the dam with a 4° flume slope at this stage. When the flume slopes were 7° and 10° , no material accumulated on the land-side slope. This difference is because the greater the slope of the flume, the greater the potential energy and the stronger the ability of the flow to scour dam material.

Larger slopes led to greater erosion in the second stage. In the third stage, the dam with the 10° flume slope was

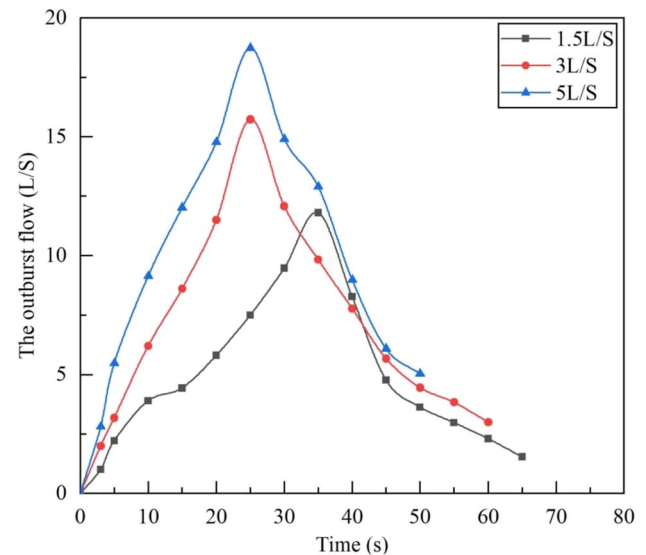


Fig. 15 Outburst flows under different upstream flow conditions (No. 2/3/5)

stable at the 40th second, and the main failure process had stopped. The dams with the 4° and 7° flume bed slopes were relatively stable at the 50th second. More residual material was observed in the dam with a 4° flume slope than in the dams with other flume slopes. The main reason for this result is that the water level in front of the dam was low in the third stage. As such, the larger the flume slope, the higher the potential energy of the water, causing the erosional effect of the water flow to be stronger. Therefore, with an increase in the flume slope, the remaining dam height decreased correspondingly.

Comparing the experiments with the different bed slopes and the same other conditions (No. 5/7/8), it was found that the greater the slope of the trench bed, the faster the rising rate of the burst flow, but the smaller the peak value of the burst flow. Comparing the outburst flow hydrographs of the different scenarios, it is found that the greater the slope of the ditch bed, the sharper the shape of the curve, but the smaller the area enclosed by the curve and the abscissa. The main reasons are that the change in the slope of the ditch bed affects both the total storage capacity of the dammed lake and the erosion capacity of the flow (Garcia et al., 2018). In addition, the greater the slope of the ditch bed, the stronger the erosion ability of the water flow, the faster the burst speed of the dam, and the faster the rising speed of the outburst flow. However, the greater the slope of the ditch bed, the smaller the storage capacity of the dammed lake, the smaller the total amount of water released by the bursting of the dam, and the smaller the peak value of the burst flow (Figs. 15 and 16).

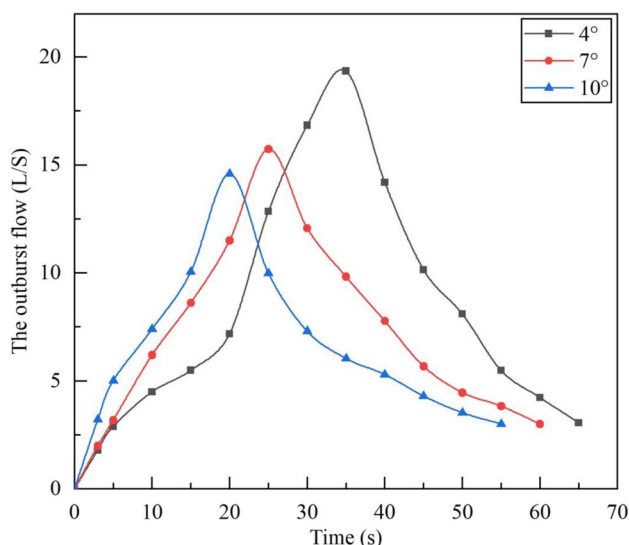


Fig. 16 The outburst flows under different bed slope conditions (No. 5/7/8)

Formula of the critical water head for an overtopping outburst

Under heavy rainfall, the water level of the dammed lake increases rapidly due to an increasing upstream inflow rate. When the water depth over the dam is high enough that the overflow velocity is greater than the critical velocity of sediment movement, the solid at the initial breach of the dam will move, and a dam failure will occur. Therefore, the dam's failure can be predicted by establishing a formula for the critical water head required for an overtopping outburst.

When analyzing the critical overflow depth of an instantaneous outburst, the critical velocity of the incipient motion of sediment should be deduced. When the influence of fine cohesion is considered, the formula of critical velocity for the incipient motion of sediment (Wu, 2008) is derived as follows:

$$v_c = \left(\frac{H}{d}\right)^{0.14} \left(17.6 \frac{\rho_s - \rho}{\rho} d + 6.05 \times 10^{-7} \frac{10 + H}{d^{0.72}}\right)^{1/2} \quad (1)$$

where v_c is the critical velocity of incipient motion of sediment (m/s), H is water head (m), d is particle size (m), ρ_s and ρ is the bulk density of solid and water. It is from Hydraulics (4th Ed.)(In Chinese). Education Press written by Wu, C.G in 2008. where $\left(\frac{H}{d}\right)^{0.14}$ is determined by the gravity of particles, $\left(17.6 \frac{\rho_s - \rho}{\rho} d + 6.05 \times 10^{-7} \frac{10 + H}{d^{0.72}}\right)^{1/2}$ reflects the viscous force between particles. The larger the particle size is, the greater the gravity effect will be. When the particle size is

reduced, the viscous force will increase. When $d > 2$ mm, the effect of viscous force can be ignored, as the starting velocity and particle size are growing relationship: $v_{c1} = \left(\frac{H}{d}\right)^{0.14} \left(17.6 \frac{\rho_s - \rho}{\rho} d\right)^{1/2}$, When $d < 0.02$ mm, the gravity effect is small, and the first term can be ignored. At this time, the relationship between the starting velocity and the particle size is negative growth: $v_{c2} = \left(\frac{H}{d}\right)^{0.14} \left(6.05 \times 10^{-7} \frac{10 + H}{d^{0.72}}\right)^{1/2}$. According to the calculation results of the two formulas, v_{c1} is suitable for the calculation of sediment initiation at the break of dam. Since Formula v_{c1} calculates the starting velocity of uniform sand, and the particle distribution in the dam is not uniform, and the starting conditions of particles with different particle sizes are different, the calculation results of Formula v_{c1} cannot be used as the critical break velocity of the dam. Therefore, based on the experimental results, formula v_{c1} is adjusted to the starting velocity formula of non-uniform sand. It can be concluded from equation v_{c1} that particle size d and water depth H are the key factors controlling sediment starting, so equation v_{c1} is adjusted as:

$$v_c = kH^{0.14} d^a \quad (2)$$

The discharge of outburst flow can be calculated as follows (Hunt 1984):

$$Q = 0.296bg^{0.5} \left(\frac{B}{b}\right)^{0.25} H_0^{1.5} \quad (3)$$

where Q is the discharge of the outburst flow, b is the width of the breach, B is the length of the dam, and H_0 is the water depth.

The initial breach is rectangular, so the flow velocity at the breach is as follows:

$$v_c = \frac{Q}{b \times H_0} = 0.296g^{0.5} \left(\frac{B}{b}\right)^{0.25} H_0^{0.5} \quad (4)$$

When the dam starts breaking, the depth of the water is equal to the water head. As such, the formula of the critical water head for an overtopping outburst can be derived:

$$H_0 = kd^a / \left[\left(\frac{B}{b}\right)^{0.694}\right] \quad (5)$$

Natural dams are broadly graded material, and the incipient motion of sediment is mainly controlled by coarse particles. Because d_{95} controls hydraulic conditions (Johnson et al. 2017), d_{95} was chosen to characterize particle size d . An exponential relationship was found between d_{95} and the measured water head, as shown in Fig. 17. This result indicates that the model established by these three independent variables can better explain the

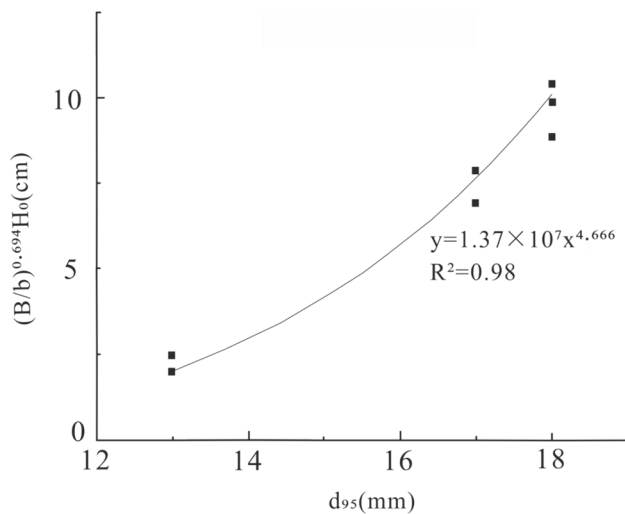


Fig. 17 Fitting curve of d_{95} and the measured head

variation of the water head. According to the fitted curve, the formula can be further changed to:

$$H_0 = 1.37 \times 10^7 d_{95}^{4.666} / \left[\left(\frac{B}{b} \right)^{0.694} \right] \quad (6)$$

The critical water head of the overtopping breach is positively correlated with the dam particle d_{95} , and d_{95} is the main influencing factor. The larger the d_{95} , the stronger the resistance to water erosion, and the larger the critical head value. The critical water head of the breach is also negatively correlated to the size of the breach and the length of the dam body.

The overtopping head h_0 is also the highest water head under the critical hydraulic condition of the dam body, it is obtained from the actual measurement during the test. Finally, formula 6 is fitted according to the actual values of h_0 and d_{95} . The formula of the critical water head for overtopping outbursts established in this paper is applied to the Baige landslide dam. The critical water head for overtopping outbursts is calculated to be 2.64 m, which is close to the actual value of 2.85 m (Xu et al., 2018). This similarity shows that the above formula of the critical water head for the overtopping outburst is consistent with reality.

Discussion

In this paper, the landslide dam in the Goulinping gully, a typical debris flow gully in a strong earthquake area of western China, was taken as the prototype. A laboratory flume device at the Institute of Geological Natural Disaster Prevention and Control of the Gansu Academy of Sciences was designed and used to conduct overtopping landslide dam

failure experiments. These experiments ignored external factors such as rainfall, hurricanes, and earthquakes. The flume was made of a steel plate at the bottom and plexi-glass on both sides. The seepage rate of the contact area between the flume and the dam body was larger than that of the natural state, meaning that the slope instability phenomenon was more obvious in the experiments than under natural conditions.

This paper studied the evolution of dam failure and flood hydrographs of the outburst flow. Due to the influence of the Wenchuan earthquake, the rock mass in the study area is relatively broken, and the source material of the dam mainly comprises non-cohesive soils and phyllite. The breach geometry and flood hydrograph of the dams are similar to non-cohesive dams (Walder et al., 2015). However, the adaptability of the experimental results to dams formed by cohesive soils remains to be discussed.

The influence of the bottom groove slope, upstream inflow, and median dam particle size on the dam failure process. Scenarios with different ditch bed slopes represent dams at different ditch positions. Scenarios with different upstream inflows represent dams at different times of the year. Scenarios with different particle configurations represent dams formed by different types of landslides. These are all the key factors affecting the erosion of the dam body. However, for the flood hydrograph of the outburst flow, some factors, such as the initial height of the dam and the shape of the dammed lake, cannot be ignored. For example, the peak discharge of the outburst flow increased almost linearly as a function of initial dam height (Walder et al., 2015). Therefore, there are many more factors to consider in the future.

Conclusion

This study conducted a series of tests to investigate the influence of multi-factors on the dam failure process. A critical water head for an overtopping outburst has been established based on the theory of the incipient motion of sediment. The main conclusions are as follows:

1. The failure mechanism of landslide dam was revealed in this study. Before the dam collapse, the existence of the notch surface accelerates infiltration and causes advancement of the speed of the wet front. The dam failure process can be divided into three stages: erosion initiation, erosion acceleration, and erosion weakening. Three important erosion phenomena were observed in the dam failure process: slope instability, steep slope, and collapse. The erosion rate first increased and then decreased along the flow direction. The maximum erosion point moved back to the source and reached a maximum value in the middle of the dam body.

2. The slope of the flume bed, the upstream inflow, and the median particle size of the dam had significant impacts on the characteristics of dam failure. The larger the median particle size, the larger the permeability coefficient. In addition, the larger the soil saturation range before the collapse, the faster the outburst flow increases and the larger the peak discharge. Finally, the larger the upstream inflow and bottom groove slope, the stronger the hydrodynamic forces, serving to increase the erosion of the dam and shorten the duration of the main collapse.
3. A critical water head for an overtopping outburst has been established based on the theory of incipient motion of sediment and experimental data. This result can be used to predict dam failure and has been verified by the Baige landslide dam.

Acknowledgements This research was supported by the National Natural Science Foundation of China (Grant Nos. 42077230 and 42130709), Gansu Province Science and Technology major Project (22ZD6FA051), important talent project of Gansu Province (2022RCXM033), and the Innovation Facility and Talent Plan Project of Gansu Province (Grant No. 20JR10RA657).

Data Availability The data that support the findings of this study are available from the corresponding author upon reasonable request.

Declarations

Conflicts of interest The authors declare no conflict of interest.

References

- Cai HJ, Liu HC, Zhang ZY et al (2001) Preliminary study on stability of natural earth-rock dam. *Geol Sci Technol Inf* 20(1):78–82 (in Chinese)
- Carrivick JL (2010) Dam break – outburst flood propagation and transient hydraulics: A geosciences perspective. *J Hydrol (amsterdam)* 380(3):338–355. <https://doi.org/10.1016/j.jhydr.2009.11.009>
- Casagli N, Ermini L, Rosati G (2003) Determining grain size distribution of the material composing landslide dams in the northern apennines: Sampling and processing methods. *Eng Geol* 69(1):83–97. [https://doi.org/10.1016/S0013-7952\(02\)00249-1](https://doi.org/10.1016/S0013-7952(02)00249-1)
- Chang DS, Zhang LM (2010) Simulation of the erosion process of landslide dams due to overtopping considering variations in soil erodibility along depth. *Nat Hazard* 10(4):933–946. <https://doi.org/10.5194/nhess-10-933-2010>
- Chen NS, Zhou W, Yang CL, Hu GS, Gao YC, Han D (2010) The processes and mechanism of failure and debris flow initiation for gravel soil with different clay content. *Geomorph (amsterdam, Netherlands)* 121(3):222–230. <https://doi.org/10.1016/j.geomorph.2010.04.017>
- Chen X, Cui P, You Y, Cheng Z, Khan A, Ye C, Zhang S (2017) Dam-break risk analysis of the attabad landslide dam in pakistan and emergency countermeasures. *Landslides* 14(2):675–683. <https://doi.org/10.1007/s10346-016-0721-7>
- Costa J, Schuster R (1988) the formation and failure of natural dams. *Geol Soc Am Bull* 100(7):1054–1068. [https://doi.org/10.1130/0016-7606\(1988\)100%3c1054:TFAPON%3e2.3.CO;2](https://doi.org/10.1130/0016-7606(1988)100%3c1054:TFAPON%3e2.3.CO;2)
- Cui P, Zhou GGD, Zhu XH, Zhang JQ (2013) Scale amplification of natural debris flows caused by cascading landslide dam failures. *Geomorph (amsterdam, Netherlands)* 182(15):173–189. <https://doi.org/10.1016/j.geomorph.2012.11.009>
- Dueck JG, Purevjav D, Kilimnik DY (2004) A Contribution to the Theory of Porosity of Fine-Grained Sediments. *J Eng Phys Thermophys* 77:93–102. <https://doi.org/10.1023/B:JOEP.0000020722.04941.c5>
- Ermini L, Casagli N (2003) Prediction of the behaviour of landslide dams using a geomorphological dimensionless index. *Earth Surf Proc Land* 28(1):31–47. <https://doi.org/10.1002/esp.424>
- Frank Penner. The maximum discharge of outburst floods caused by the breaching of man-made and natural dams: Discussion. *Canadian Geotechnical Journal*. 24(3): 469–469. <https://doi.org/10.1139/t87-061>
- Hakimzadeh H, Nourani V, Amini AB (2014) Genetic programming simulation of dam breach hydrograph and peak outflow discharge. *J Hydrol Eng* 19(4):757–768. [https://doi.org/10.1061/\(ASCE\)HE.1943-5584.0000849](https://doi.org/10.1061/(ASCE)HE.1943-5584.0000849)
- Hunt, B. (1984). Dam-break solution. *J Hydraul Eng (New York, N.Y.)*, 110(6), 675–686. [https://doi.org/10.1061/\(ASCE\)0733-9429\(1984\)110:6\(675\)](https://doi.org/10.1061/(ASCE)0733-9429(1984)110:6(675))
- Iqbal, J., Dai, F., Xu, L., & Xinbin, T. (2013, April). Characteristics of large-sized landslide dams around the World. In *EGU Gen Assem Conf Abstr* (pp. EGU2013–256)
- Jiang X, Zhanyuan Z, Chen H, Deng M, Niu Z, Deng H, Zuyin Z (2020) Natural dam failure in slope failure mode triggered by seepage. *Geomat Nat Haz Risk* 11(1):698–723. <https://doi.org/10.1080/19475705.2020.1746697>
- Johnson, J. P. L., K. Delbecq, and W. Kim. (2017). Predicting paleo-hydraulics from storm surge and tsunami deposits: Using experiments to improve inverse model accuracy. *J. Geophys. Res. Earth Surf.*, 122, 760–781. <https://doi.org/10.1002/2015JF003816>
- Korup O (2002) Recent research on landslide dams - a literature review with special attention to New Zealand. *Prog Phys Geogr: Earth Environ* 26(2):206–235. <https://doi.org/10.1191/0309133302pp333ra>
- Li Y, Wang BL, Zhou XJ, Gou WC (2015) Variation in grain size distribution in debris flow. *J Mt Sci* 12(3):682–688. <https://doi.org/10.1007/s11629-014-3351-3>
- LUKAS SCHMOCKER and WILLI H. HAGER. (2010). Modelling dike breaching due to overtopping. *Journal of hydraulic research. J Hydraul Res*, 48(4), 547–549. <https://doi.org/10.1080/00221686.2010.492097>
- Peng M, Zhang LM (2012) Breaching parameters of landslide dams. *Landslides* 9:13–31. <https://doi.org/10.1007/s10346-011-0271-y>
- Shen D, Shi Z, Zheng H, Yang J, Hanley KJ (2022) Effects of grain composition on the stability, breach process, and breach parameters of landslide dams. *Geomorphology (amsterdam, Netherlands)* 413:108362. <https://doi.org/10.1016/j.geomorph.2022.108362>
- Shu AP, Wang L, et al. (2017). Study on the Formation and Initial Transport for Non-Homogeneous Debris Flow. *Water*. 9(4):253. <https://doi.org/10.1109/TALE.2014.7062632>
- Smith HE, Monsalve AD, Turowski JM, Rickenmann D, Yager EM (2023) Controls of local grain size distribution, bed structure and flow conditions on sediment mobility. *Earth Surf Proc Land* 48(10):1990–2004. <https://doi.org/10.1002/esp.5599>
- Takahashi T (2007) Debris flow: Mechanics, prediction and countermeasures. Taylor & Francis Group Press. <https://doi.org/10.1007/s00024-008-0342-8>

- Wasowski J, McSaveney MJ, Pisano L, Del Gaudio V, Li Y, Hu W (2021) Recurrent rock avalanches progressively dismantle a mountain ridge in Beichuan County, Sichuan, most recently in the 2008 Wenchuan earthquake. *Geomorphology* 374:107492. <https://doi.org/10.1016/j.geomorph.2020.107492>
- Xu F, Yang X, Zhou J, Hao M (2013) Experimental research on the dam-break mechanisms of the Jiadanwan landslide dam triggered by the Wenchuan earthquake in China. *Sci World*. <https://doi.org/10.1155/2013/272363>
- Yang Y, Cao S Y. (2012) Experimental study on failure mechanism of dam. *J Hydraul Eng*,43(S2):60–67. (in Chinese)
- Zhou M Y et al. (2019a) Influence of inflow discharge and bed erodibility on outburst flood of landslide dam. *J Mt Sci*, 16(4): 778–792. <https://doi.org/10.1007/s11629-018-5312-8>
- Zhou GGD, Zhou M, Shrestha MS, Song D, Choi CE, Cui KFE, Peng M, Shi Z, Zhu X, Chen H (2019b) Experimental investigation on the longitudinal evolution of landslide dam breaching and outburst floods. *Geomorphology (Amsterdam, Netherlands)* 334:29–43. <https://doi.org/10.1016/j.geomorph.2019.02.035>
- Zhou, G. G. D., Lu, X., Xie, Y., Cui, K. F. E., & Tang, H. (2022). Mechanisms of the Non-Uniform breach morphology evolution of landslide dams composed of unconsolidated sediments during overtopping failure. *J Geophys Res. Earth Surface*, 127(10), n/a. <https://doi.org/10.1029/2022JF006664>
- Zhu X, Peng J, Jiang C, Guo W (2019) A preliminary study of the failure modes and process of landslide dams due to upstream flow. *Water* 11(6):1115. <https://doi.org/10.1029/2022j006664>
- Zhu YH, Visser PJ, Vrijling JK et al (2011) Experimental study on dam break. *Chinese Sci : Technol Sci* 41(2):150–157 (in Chinese)